PART 3: CASE STUDY

CHAPTER 5

LITERATURE SURVEY

This chapter covers a literature survey relating to the case study. A description of the case study is given in chapter 1. Transverse cracking in turbine rotors is not a very common phenomenon, presumably as a result of good design, but a number of incidences have been reported in open literature. It would be good practise to relate structural integrity studies to industry experience.

Structural integrity of components with known degradation mechanisms alsorelies on inspection and monitoring techniques for safe operation. The basics of non-destructive testing on the turbines are covered briefly. As discussed earlier, on-line monitoring plays an important role in preventing catastrophic failure, and this topic is covered in more detail.

The last section covers a literature survey on the material properties of rotor steel. The accuracy of calculated parameters and associated assumptions can be controlled to some degree. These parameters must however be related to the material properties of the actual component. It is not possible to perform material tests on the component while it is in service so that one has to rely on researched results and general experience in the field of materials technology to derive appropriate material properties.

5.1 INDUSTRY EXPERIENCE

Viswanathan and Jaffee published a list of known steam turbine shaft failures [P1]. The study covers dates from 1954 to 1985. Of the 35 failures, 24 occurred in LP turbines.

Of the 24 LP failures, transverse cracking caused 16 of which 12 cases were detected by shaft vibration. Of the 4 cases where cracking was not detected by vibration monitoring, 2 had relatively small cracks while no direct references are available on case studies for the other 2 cases. Table 5.1 gives comparative information on the occurrence of transverse cracking in the 16 recorded cases as well as literature references where available.

The following aspects from the reported failures are of specific interest:

- The cracks are located near regions of high stress and generally initiate in corrosion pits [P1].
- A number of references [P1,P6,P7,P8] recognise the inadequacy of materials fatigue data for dry and wet/dry steam conditions.
- Finite element analysis on rotors with shrunk on disks showed that the risk of crack initiation is greatest when the turbine was rotating at barring speed [P7,P9]. This is confirmed by correlating the beach marks on the crack surface to the operating history of the shafts.
- The increased vibration levels were not attributed to the existence of a crack. Major attempts were made to "balance out" the vibration problem before the shaft was inspected for crack detection [P11].

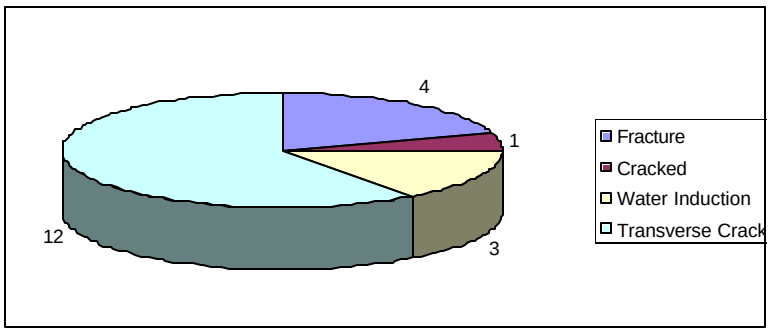

Figure 5.1: Incidence of turbine failure

Plant Name	Vibration (Y/N)	Size** [%]	Ref.
Wurgassen (x2)	Y	25.1	P7
Ferrybridge C (x3)	Y	19.9	P7,P8
R. S. Wallace	Y	*25	P7
Fort Martin (x2)	Y	NA	P7
USA	Y	*30	P9
USA	Y	*80	P9
USA	Y	17.5	P10
Waukegan	Y	27.4	P11
St. Clair	NA	NA	NA
Pennelec/Shawville	N	*17	P12
State	N	*13	P11
Campbell	NA	NA	NA

Table 5.1: Failed LP turbine shafts by transverse cracking
* Best estimate
** Percentage of shaft diameter
NA = Not Available

5.2 NON-DESTRUCTIVE TESTING

While fatigue and fracture assessment of a component are invaluable tools in the management of defected structures, the problem only arises once the defect is identified by inspection. If the inspection technique can determine some flaw characteristics such as shape and size, effective analysis becomes a realproposition in determining the future use of the component, whether it is maintenance, continued use or retirement.

To this end, non-destructive testing forms an essential and integral part of structural analysis. It is also important to come to grips with the reliability and accuracy of the techniques. Although NDT is not a primary part of this work, a brief discussion is presented for completeness.

5.2.1 Inspection Techniques

Non-destructive testing (NDT) deals with inspection techniques that interrogate a component with the aim of detecting anomalies such as cracks. In general, NDT can be divided into three categories namely:

- electromagnetic
- penetrant
- acoustic

Electromagnetic techniques rely on the disturbance in the magnetic field caused by anomalies in a magnetised component. The disturbance can be recorded by electromagnetic receivers, eddy current testing, or by visual aids, magnetic particle testing.

Penetrant techniques rely on a dye to penetrate defects or cracks in the structure. The excess dye is cleaned off and the crack is visible as a result of dye seeping out of the crack cavity. Penetrant techniques are often enhanced by the use of fluorescence.

Acoustic techniques rely on the propagation of sound waves travelling through the component and can be divided in two main classes namely acoustic monitoring and ultrasonic testing. In acoustic monitoring, an active crack is required for detection. When an incremental crack extension occurs, the energy release causes a mechanical wave to propagate through the structure. The mechanical wave can be detected by piezoelectric crystals.

Ultrasonic testing is performed by generating and transmitting an ultrasonic wave into the component. Scatter, diffraction, reflection or other wave phenomenon modifies the wave when it encounters anomalies. A suitably placed piezoelectric crystal in turn receives the sound wave and interpretations can be made about anomalies in the structure.

Ultrasonic testing (UT) is by far the most popular NDT technique and has the advantage that it can interrogate a volume. Electromagnetic and penetrant techniques can only be used to inspect the surface layer of the component and requires direct access to the inspection surface. Such direct access is not possible in the case study under investigation, see figure 1.1 to 1.3 at the end of chapter 1.

5.2.2 Ultrasonic Testing

UT has a vast field of application and is often very disciplined in specific fields. The primary variables in UT are amplitude and time. The transmitted signal is of little importance other than to have the correct characteristic, such as power, frequency etc., to penetrate the component and to respond to the expected anomalies. The received signal is recorded as an amplitude-time trace.

Some techniques rely almost entirely on the amplitude of the sound wave reflected from, or shielded by, an anomaly, some take the time-space trace (i.e. the compounded signal trace of all recordings taken from different positions on the component) of the signal into consideration to determine characteristics of the anomaly. The pulse-echo and through transmission techniques are examples of these (figure 5.2).

The time-of-flight-diffraction (TOFD) technique in turn relies almost entirely on the time base information to interpret the nature of anomalies. The amplitude is only of importance to identify acoustic incidences in the received signal. TOFD is generally

recognised as the most accurate technique for determining the physical size of cracks (figure 5.3). A number of graphic display standards were developed over the years to enhance the presentation of data and to assist in the interpretation of signals.

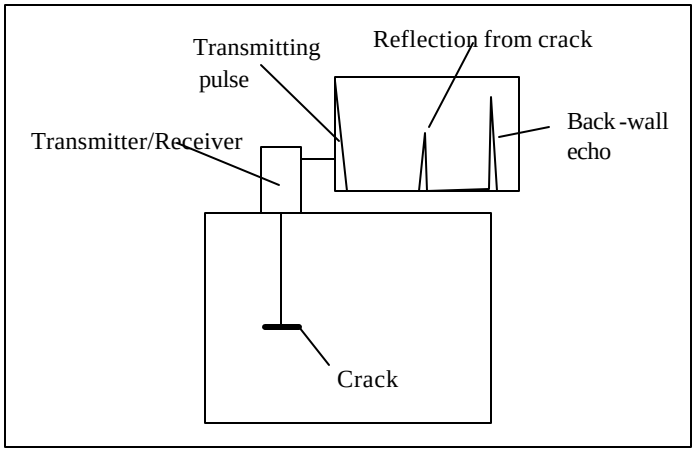

Figure 5.2: Schematic of pulse-echo technique

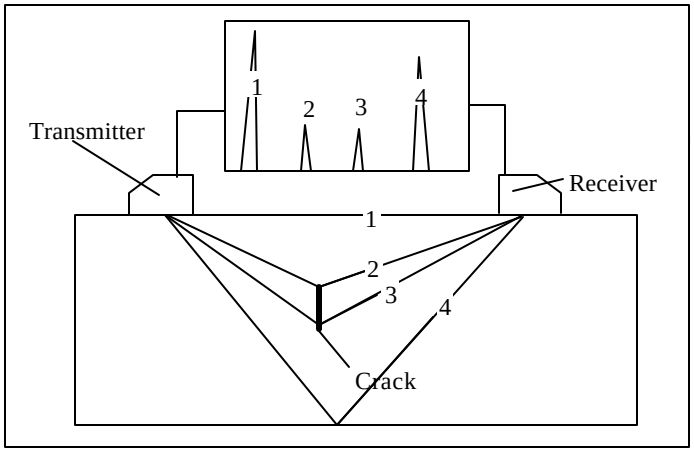

Figure 5.3: Schematic of TOFD technique

5.2.3 Turbine Shaft Inspection [U1]

The turbine shaft in figure A.1 was historically inspected by the pulse-echo technique from the bearing surfaces. The purpose of shaft inspections was to detect cracking from possible manufacturing defects and from the fillet areas on the rotor surface.

The pulse-echo technique, see figure 5.4, requires the sound to travel from the end of the shat to the middle and back. The beam spread of an ultrasonic sound wave over such a long path is considerable. Although the key area never formed part of the inspection scope, it was geometrically covered by the beam spread.

When the suspicion of cracking from the key came to light, further evaluation of the ultrasonic signals gathered during historical inspections, confirmed the incidence of cracking on a number of rotors. The technique is, however, not ideally suited for sizing because of the long sound path and beam spread so that the initial estimates on crack size were grossly overestimated. Sound reverberations around the various facets in the key have a further detrimental effect on the reliability of detection.

The seriousness of the problem initiated urgent investigations to come up with a technique that would provide reliable and accurate sizing. Initial investigations proved that the interference fit interface, between the disks and shaft, have sufficient transparency for inspection purposes.

A third party inspector was contracted to develop a TOFD procedure for this application. The procedure was applied and successful sound transmission through the interfaces could be proven, because the various key facets and relatively small cracks could be detected.

In parallel to the development of the aforementioned TOFD technique, the original equipment manufacturer (OEM) initiated the development of a second TOFD technique, applied from the shaft ends. Although focussed probes were used (smaller beam spread), the large probe separation is not ideal for accurate TOFD sizing. Figure 5.4 shows a schematic of the 3 techniques discussed.

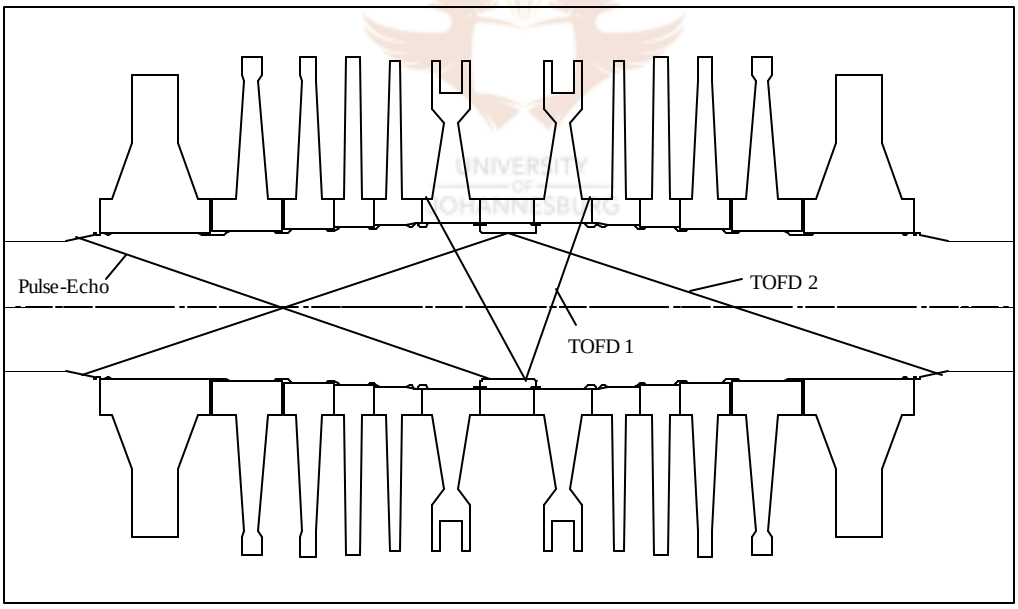

Figure 5.4: Schematic of ultrasonic techniques

TOFD 1, in figure 5.4, is expected to have a sizing accuracy of ± 1 mm, while TOFD 2 is reported to have a sizing accuracy of ± 5 mm. The inspections, for the shafts used in the case study, revealed a maximum crack size of 15.4 mm which is less than the depth of the key.

5.3 VIBRATION MONITORING

Vibration monitoring, like NDT, is not a primary part of this work, but also forms a vital component of the overall assessment process. A turbine shaft with a known defect can only be operated if there is a very high level of confidence that evolution of the defect will be detected at an early stage i.e. well before a catastrophic failure is imminent.

5.3.1 General Discussion [P17]

It is evident, from the amount of available literature, that crack detection by vibration monitoring is an active research topic. Computational models for rotor dynamic analysis are also hampered by a number of uncertainties like bearing stiffness, damping etc. It is imperative to calibrate a rotor dynamic model to measurements before it is used in a predictive mode.

Three approaches to rotor crack detection were found in open literature namely:

- Coast down
  The coast down approach relies in the change in natural frequency when a crack is present. A machine is taken offline and decelerated while the vibration spectrum is determined as a function of speed. The change in natural frequency results in a change in the critical speed, which is measured and used for crack detection. The coast down approach seems to be the most popular, judging on the number of published papers.
- Temperature transient
- On-line

A steady state on-line approach is required for the case at hand. The dynamics of the basic problem would be the same for other rotors so that an on-line approach would be the preferred one for all crack detection in components subjected to high frequency cyclic loads.

All three approaches are discussed in the survey, because they trend the development of rotor dynamic models for crack detection and give valuable insight into the theory applied to later models.

As mentioned earlier, the rotors have three keys, spaced at equal angles of 120 ° around the circumference, in the centre of the rotor. Cracks initiate by fretting and propagate from the keyways.

A crack, emanating from a keyway, will result in a “breathing” crack. Such a crack is described as breathing because of the opening-closing cycle that it undergoes as the shaft rotates in bending. Figure 5.5 is a graphical presentation of the change in the effective second moment of area (or stiffness) as a shaft, with a single crack, goes

through one revolution. The shaft deflection will vary in a similar fashion, but will be out of phase with the stiffness.

A shaft, subjected to bending moment under its own weight, has a compressive stress at the top. When the crack is on top, it is in a closed state and the presence of the crack has no influence on the stiffness characteristics of the shaft. The stiffness decreases as a part of the crack rotates to the bottom halve of the shaft, which is in tension. The crack opens when it is at the bottom of the shaft with a resulting decrease in the effective sectional properties and stiffness of the shaft. This opening-closing cycle is termed "breathing" of the crack.

Asymmetric stiffness fluctuation is the strongest excitation mechanism for vibration due to transverse cracks in a rotation shaft. An asymmetric stiffness matrix results in coupling between modes so that model for an uncracked shaft is no longer valid. Also, the deeper the crack, the larger the asymmetric terms.

While it is accepted that the shaft may not respond at its natural frequency if no amplification factor exist, the forcing function will become higher as the crack propagates and will ultimately become significantly non-linear. This, together with coupling of modes should be fully investigated before crack detection by vibration monitoring can be discarded as not possible.

No steam turbine is designed to run at speeds where high amplification factors exist, yet there are many recorded instances where a unit was shut down due to excessive vibration levels, resulting from large cracks.

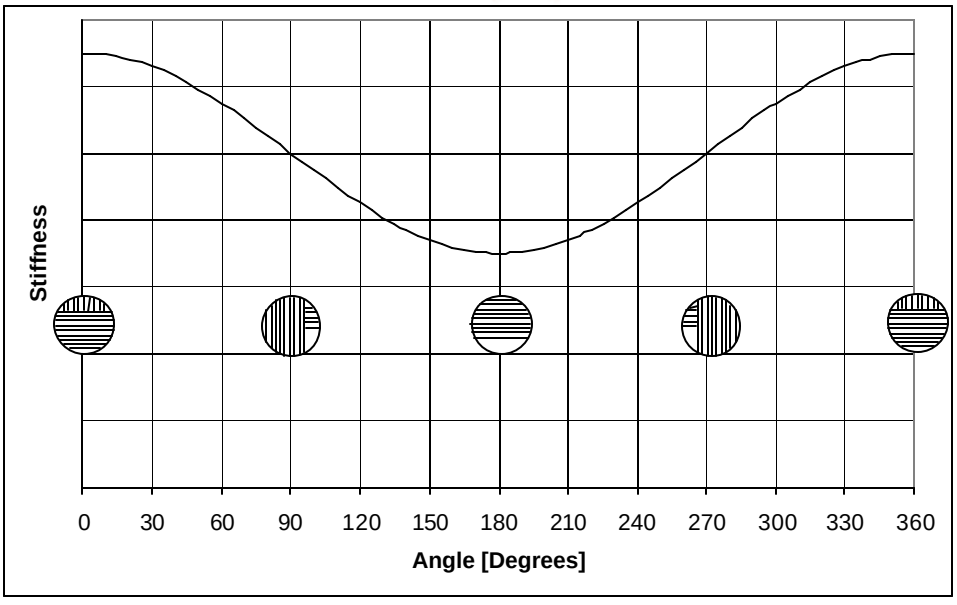

Figure 5.5: Stiffness fluctuation with rotation for a cracked shaft

There is a possibility that cracks can simultaneously grow from all three keyways and form a continuous symmetric crack when it is still relatively shallow. Experience so far has shown that this possibility is rare, but the early life of cracks can be effectively monitored by non-destructive testing to see if this is the case [U1]. A symmetric crack will result in a symmetrical lowering of the stiffness and not a fluctuation as shown in figure 5.5.

5.3.2. Early Developments

The usefulness of crack detection by vibration monitoring was recognised in the mid 1970s and the first work was done by the General Electric Company. The work introduced the bending stiffness description of a rotor crack [P17].

Most of the early work, as well as some recent developments, use the so-called de Laval type rotor, which consists of a single rigid disk mounted on a simply supported shaft with a negligible mass. Although the model is not the same as a rotor train system, or even a complex single rotor, valuable insight and theoretical developments resulted from the simplifications.

Subsequent to the initial work, a number of researchers introduced a stiffness change due to a crack into the equations of motion. Gash [P18] developed a model based on a displacement controlled spring mechanism with a step function for open and close conditions, introducing the "breathing" concept.

The step change in stiffness was introduced by defining a flexibility matrix, $\underline{\mathbf{H}}$, in rotating Cartesian co-ordinates, $\underline{\mathbf{x}}$ with displacements ζ and η, as follows:

$$\begin{bmatrix} \zeta \\ \eta \end{bmatrix} = \begin{bmatrix} h^W + h^F & 0 \\ 0 & h^W \end{bmatrix} \begin{bmatrix} F_\zeta \\ F_\eta \end{bmatrix} \qquad (5.3.1)$$

or $\underline{\mathbf{x}} = \underline{\mathbf{H}}.\underline{\mathbf{F}}$

where h^W is the shaft flexibility and h^F is a step function of the additional crack flexibility while F_ζ and F_η are the force components (see figure 5.6). Underline indicates that the rotating co-ordinate system is used. The crack flexibility, h^F was defined as follows:

$$h^F = 0 \text{ for } F_\zeta < 0 \text{ i.e. } \zeta < 0$$
$$h^F > 0 \text{ for } F_\zeta > 0 \text{ i.e. } \zeta > 0 \qquad (5.3.2)$$

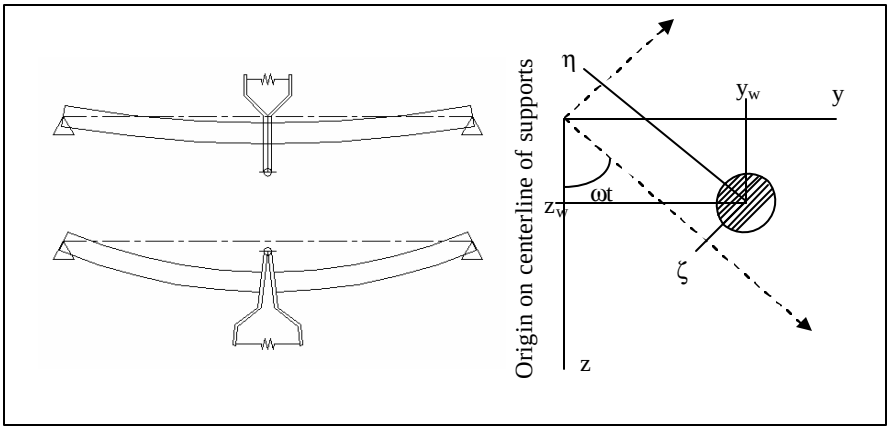

Figure 5.6: Gash's crack model and co-ordinate axis

Assume a constant angular velocity of ω, the angular rotation of the axis is ωt where t is the time. Equation 5.3.1 can be written in an equivalent form, as used in a stiffness formulation as:

$$\begin{bmatrix} k_{\zeta\zeta} & k_{\zeta\eta} \\ k_{\eta\zeta} & h_{\eta\eta} \end{bmatrix} \begin{bmatrix} \zeta \\ \eta \end{bmatrix} = \left\{ \begin{bmatrix} c_w & 0 \\ 0 & c_w \end{bmatrix} - \begin{bmatrix} \Delta c(\zeta) & 0 \\ 0 & 0 \end{bmatrix} \right\} \begin{bmatrix} \zeta \\ \eta \end{bmatrix} = \begin{bmatrix} F_\zeta \\ F_\eta \end{bmatrix} \qquad (5.3.3)$$

or $\underline{\mathbf{Kx}} = \underline{\mathbf{F}}$

with $c_w = 1/h_w$
$\Delta c = 0$ for $\zeta < 0$
$\Delta c = (1/h_w)[1/(1+h_w/h_f)]$ for $\zeta > 0$

Components of the stiffness matrix in equation 5.3.3 are obtained by the inverse of the flexibility matrix in equation 5.3.1 and are non-linear according to the relations in equation 5.3.2.

The general equation of motion for a rotating shaft is (in matrix notation)

$$\mathbf{M\ddot{x} + D\dot{x} + Kx = g + \varepsilon t} \qquad (5.3.4)$$

with **M** = Mass matrix
D = Damping matrix
K = Stiffness matrix or inverse of flexibility matrix ($\mathbf{K} = \mathbf{H}^{-1}$)
g = Gravity matrix
e = Eccentricity matrix

All matrices, except for the fluctuating stiffness and the eccentricity vector, are derived in the fixed co-ordinate system. The eccentricity matrix can be derived in the

rotating co-ordinate system by considering the distance from the centreline of the rotor to its centre of gravity and the angle, β, of the unbalance relative to the ζ-axis.

Equation 5.3.3 and the eccentricity matrix must be transformed to the fixed co-ordinate axis by a standard transformation matrix, for inclusion in the equation of motion, as follows:

$$\mathbf{F} = \mathbf{T}^{-1}.\underline{\mathbf{F}},\ \mathbf{x} = \mathbf{T}^{-1}.\underline{\mathbf{x}} \text{ and } \mathbf{K} = \mathbf{T}^{-1}.\underline{\mathbf{K}}.\mathbf{T}$$

with
$$\mathbf{T} = \begin{bmatrix} \cos(\Omega t) & -\sin(\Omega t) \\ \sin(\Omega t) & \cos(\Omega t) \end{bmatrix} \tag{5.3.5}$$

Assembly of all components into the equation of motion (5.3.4) yields:

$$\begin{bmatrix} m & 0 \\ 0 & m \end{bmatrix}\begin{bmatrix} \ddot{z} \\ \ddot{y} \end{bmatrix} + \begin{bmatrix} d & 0 \\ 0 & d \end{bmatrix}\begin{bmatrix} \dot{z} \\ \dot{y} \end{bmatrix} + \begin{bmatrix} k_{zz} & k_{zy} \\ k_{yz} & k_{yy} \end{bmatrix}\begin{bmatrix} z \\ y \end{bmatrix} = \begin{bmatrix} mg \\ 0 \end{bmatrix} + \varepsilon\Omega^2\begin{bmatrix} \cos(\Omega t + \beta) \\ \sin(\Omega t + \beta) \end{bmatrix} \tag{5.3.6}$$

where *b* is the phase angle of the eccentricity.

The components of the stiffness matrix, k_{ij}, are functions of time, t, in the fixed co-ordinate system. The solution routine, employed by Gash, required equation 5.3.6 to be transferred to the rotating co-ordinate system. The advantage of such a transformation is that the equation of motion is no longer time variant, except for gravity. The transformation process is similar to what was described earlier, but noting the following in relation to differentiation rules:

$$\begin{aligned} \dot{\mathbf{x}} &= \dot{\mathbf{T}}^{-1}\underline{\mathbf{x}} + \mathbf{T}^{-1}\underline{\dot{\mathbf{x}}} \\ \ddot{\mathbf{x}} &= \ddot{\mathbf{T}}^{-1}\underline{\mathbf{x}} + 2\dot{\mathbf{T}}^{-1}\underline{\dot{\mathbf{x}}} + \mathbf{T}^{-1}\underline{\ddot{\mathbf{x}}} \end{aligned} \tag{5.3.7}$$

The equations of motion in rotating co-ordinates are:

$$\begin{bmatrix} m & 0 \\ 0 & m \end{bmatrix}\begin{bmatrix} \ddot{\zeta} \\ \ddot{\eta} \end{bmatrix} + \begin{bmatrix} d & -2m\Omega \\ 2m\Omega & d \end{bmatrix}\begin{bmatrix} \dot{\zeta} \\ \dot{\eta} \end{bmatrix} + \left\{\begin{bmatrix} (c_w - \Omega^2 m) & -\Omega d \\ \Omega d & (c_w - \Omega^2 m) \end{bmatrix} - \begin{bmatrix} \Delta c(\zeta) & 0 \\ 0 & 0 \end{bmatrix}\right\}\begin{bmatrix} \zeta \\ \eta \end{bmatrix}$$

$$= mg\begin{bmatrix} \cos(\Omega t) \\ -\sin(\Omega t) \end{bmatrix} + \varepsilon^2 m\Omega^2\begin{bmatrix} \cos(\beta) \\ \sin(\beta) \end{bmatrix} \tag{5.3.8}$$

Gash [P18] produced graphs with normalised parameters of the solutions to his model. The graphs show a strong vibration response at 1/2 critical speed, but also at approximately 1/3 and 2/3 of the critical speed which is claimed as a characteristic of the cracked shaft model (compared to an uncracked shaft or a shaft with unequal stiffness).

All the publications that were found on analytical research work, for the shaft crack problem, are based on a similar two degree-of-freedom formulation of the de Laval rotor. Various normalisation schemes were employed for the time and displacement terms to simplify analysis.

Henry [P19] derived the equations of motion for a model with shaft stiffness asymmetry. The resulting equations are similar to equation 5.3.8 without the Δc term and with different stiffness coefficients for the different co-ordinate axis directions. The asymmetry in the shaft stiffness is such that there are two perpendicular symmetry axes as would be the case for a rectangular or elliptical shaft. Such a shaft would be similar to a round shaft with transverse cracks separated by 180°. A shaft with asymmetric stiffness will have a twice per revolution excitation, while a shaft with a single crack has a synchronous excitation.

Henry [P19] compared his rotor dynamic model to experimental results on shafts that were designed with asymmetric stiffness and reports very good correlation. There are a number of similarities between asymmetric and cracked shafts, some of which were reported by Gash [P18]. Henry [P19] reports that:

- Both cases have strong responses at 1/2 critical speed.
- Only the cracked shaft exhibits resonant response at odd fractions i.e. 1/3 and 1/5 of the critical speed.
- The path of whirl for resonance at subcritical speed is dependent on the amount of eccentricity.
- The eccentricity dominates asymmetric stiffness effects at speeds above the critical speed so that the crack detection is not possible for angular velocities above the critical speed.

Henry [P19] concludes that a coast down approach is suitable for crack detection and reports on a case where it had been successfully applied on a CEGB machine.

Mayes and Davies [P20] also developed a model of a de Laval rotor. The model is derived from energy principles, to calculate the crack compliance, and uses a number of stress intensity and strain energy solutions from other sources, which are not currently available. The paper shows a large number of approximations, the effect of which could not be estimated with the information available.

Mayes et al considered the non-linear equations of a de Laval rotor, the analytical solutions were obtained for an open crack. This will produce the result for a rotor with dissimilar moments of area in perpendicular directions.

The following is summarised from reference P20:

- The axial position of the crack is important in determining its effect on the natural frequency of any particular mode. This implies that the effect is also present on the higher modes (opposed to Henry's conclusion).
- The shaft speed at which the crack has the largest effect on the vibration behaviour depends on the axial position of the crack.
- If the change in natural frequency of at least two normal modes is known, the axial position and the size of the crack can be calculated.
- The vibration behaviour of a cracked shaft depends on the phase of the out of balance.

Mayes [P20] applied the techniques to a CEGB rotor and, after some trial and error with a coast down approach and static measurements, managed to fit a successful prediction to the model.

5.3.2. Advances In The 1980s

A considerable amount of development and research were conducted in the field of crack detection by vibration monitoring in the 1980s, but Wauer [P17] reports that very little development realised from 1980 to 1990. Research in the 1980s was led by a number of groups including Dimarogonas and Papadopoulos [P21,P22,P23], Grabowski and Muszynska [P24] through the Bentley Corporation.

Although none of Grabowski's papers could be sourced, Dimarogonas et al report [P21,P25] that Grabowski argues that the deflection of shafts due to vibrations is much smaller than the deflection due to its own weight. Grabowski suggests that the non-linearity, as introduced by Gash [P18], does not affect the shaft response since the crack opens and closes regularly with rotation. This means that the equations of motions can be considered linear with variable coefficients to allow analytical solutions. The alternative is numerical integration.

Dimarogonas [P21] started off by deriving compliance coefficients (see the work by Gash) using energy principles in a two degree of freedom system. Accepting Grabowski's assumption (see above), equations were derived for uncoupled vibration of a de Laval rotor (bending degrees of freedom only). Assumptions of an open crack led to analytical solutions for a shaft with dissimilar moments of inertia and a characteristic bounded response at approximately half the critical speed. Assumptions of a breathing crack were handled analytically by time varying flexibility coefficients in the equations of motion.

Dimarogonas [P21] summarised research experience to date (1983), for a breathing crack, as follows. A slotted shaft or a shaft, equivalent to a shaft with dissimilar moments of inertia, has two speeds at which the synchronous response becomes unbounded. A breathing crack with the out-of-balance in phase with the crack has a range of speeds where the equations of motion have no solution. An out-of-balance that is out of phase has a range of speeds at which the equations of motion have two solutions of which one is unstable. Disturbances in the system would cause switching from one solution to the other, a phenomenon that is characteristic of non-linear systems.

Dimarogonas [P21] imposed compatibility conditions at the half and full cycle conditions to derive equations of motion for a breathing crack. He mapped the solution to the homogenous equation on a graph to show areas of instability. The graph confirms that there are many sub-harmonics at which instability occurs, depending on crack depth. Although the equations for the forced response were derived, no solutions were obtained. The equations indicate that the non-homogenous solution will also have a series of sub-harmonic responses.

Further work by Papadopoulos and Dimarogonas [P22] uses a stiffness formulation to describe a general 3D frame element with 6 degrees of freedom, as would be used in a finite element formulation. The compliance matrix for the localised crack effects is calculated with the aid of energy principles and incorporated into the compliance matrix for a general frame element. The stiffness matrix is found by the inverse of the compliance or flexibility matrix.

The equations of motion, derived from the formulation of a general frame element, are applied to a de Laval rotor with a crack. Since the mass is lumped in the centre of the rotor, only three degrees of freedom were used namely bending in the two principle directions and axial extension.

The analysis results show substantial coupling between the vibration modes associated with the three degrees of freedom, characterised by off-diagonal terms in the flexibility matrix. Reference P22 concludes that longitudinal vibration is associated with low levels of noise so that on-line monitoring can easily detect cracks with depth ratios of as little as 0.1 (crack depth to shaft diameter).

A third paper by Papadopoulos and Dimarogonas [P23] repeats the basics of reference P22 and includes a case study. A 300 MW ALSTHOM turbine at Lavrion in Greece experienced high vibration in 1983. Subsequent inspections revealed a crack that spanned 120 ° of the rotor circumference. Papadopoulos et al used recorded vibration signals to analyse the problem. The vibration signal showed high amplitudes at ½, ¼, and 2 per revolution frequencies. A succession of 44, 88, 176 Hz frequencies, which were later identified as sub-harmonics of the axial natural frequency, was also found. The paper concludes that coupling between vibration modes were confirmed in practice and that vibration techniques can be effectively used for crack detection in turbine shafts.

Papadopoulos and Dimarogonas further investigated coupling effects in a stationary shaft in reference P24. In this work, an open crack was assumed. The paper concludes that crack depth ratios of 0.2 and above show clearly detectable coupling.

Although a number of papers by Muszynska and Bentley were found in references in other papers, only one paper by Muszynska, working from the Bently Navada Corporation, could be obtained. The work may be of particular interest since Eskom purchased a Bently system for vibration analysis on the rotor in question.

Muszynska [P26] used a de Laval rotor for modeling and experimental work. The paper investigates the influence of elasticity unbalance, eccentricity, stiffness ratio and support stiffness for free and forced vibrations. Muszynska focused on the synchronous and two per revolution vibration signals. The paper concludes that a crack causes an increase in vibration amplitudes through the whole range of rotation speeds, but that the highest sensitivity is naturally obtained in resonant conditions.

Bentley and Muszynska [P27] report that shaft cracks can be detected by the monitoring of the specific dynamic behaviour of shafts, and analysing its evolution with time. The paper states, in the introduction, that the crack detection methods are enhanced if transient data is available, implying that steady-state online data can be used. Changes in the synchronous (1x) vibration amplitude or phase are cited as the most reliable crack evolution indicator at operating speed. Reference P27 states that changes in the 2x running speed vibrations may or may not occur depending on the specifics of the machine, but does not elaborate on the conditions under which the phenomenon change. The paper does, however, refer to vertical shafts where there is no guaranteed lateral force (gravity in the case of horizontal machines).

Bentley and Muszynska [P27] propose a mode shape prediction technique as part of the overall assessment process. The Bently Navada presentation [U2] does not include a similar technique, but the modelling assumptions are not valid in any case and do not compare with any crack assumptions found throughout the literature. Although it is possible the technique is no longer in use, more recent work follows the same trend [P30,P34,P37].

The first report of a finite element formulation to the shaft crack problem, was found in reference P28. Nelson and Nataraj [P28] modelled a breathing crack by a switching function, incorporated into the element stiffness matrix. The switching function is dependent on the bending curvature of the shaft so an iterative solution procedure had to be programmed to solve the equations. Good correlation with earlier work, including Grabowski and Henry, is reported.

Scheibel et al, working from EPRI, report on an expert system for on-line crack detection in steam turbines [P29]. The paper covers no theoretical treatment of rotor crack models, but focuses on practical implementation of diagnostic vibration systems and introduces signal processing to enhance vibration signals. The system uses most

concepts discussed in references P17 to P28 and aims to detect changes in vibration signatures, including sub-harmonics, which are used for crack detection and other rotor dynamic problems. Scheibel claims the crack depth detection threshold is 1 to 5 % of the rotor diameter, but it is not stated whether this threshold is applicable to steady-state, coast-down or temperature transient assessment.

A second paper by Scheibel et al [P30] claims their system is generically applicable to all rotors subjected to a bending load and can detect incipient transverse cracks in an on-line mode. The paper reports on a special crack element that is based on time varying load, to account for the change in deflection of the breathing crack. The element is used in 3D finite element analysis and in a non-linear rotor dynamics code. Although the modelling activities gave valuable insight to the diagnostics of cracked shafts, the success of on-line detection lies in the histogram signature analysis technique. The technique is based on the following three steps:

1. Synchronously sum the time-domain vibration data using a 1/rev reference signal as a base line signal.
2. Repeat step 1 periodically for crack monitoring purposes.
3. Subtract steps 1 and 2 in the time domain and convert the difference to the frequency domain to obtain the "histogram harmonics".

The technique was extensively validated in large scale laboratory tests and proved capable of detecting transverse cracks of approximately 1 to 2 % of the shaft diameter.

In conclusion, most research work in the 80s focussed on analytical models. Although the work gives valuable insight into some influencing parameters, it is limited, by complexity, to de Laval type rotors. Work in the 80s is marked by disagreement relating to the influence of unbalance. The first breakthrough in real life monitoring appears to be the pragmatic approach by Scheibel et al [P29,P30].

5.3.3. Advances In The 1990s

The literature survey shows that most work in the 90s concentrated on advanced analysis techniques and very little is reported on practical fieldwork. The analysis techniques, mostly numerical techniques based on a finite element formulation, allow the treatment of distributed parameter shafts, opposed to the de Laval rotor.

Wauer [P31] derives the boundary value problem for a cracked shaft and replaces the geometric discontinuity by a load discontinuity. The problem is numerically solved for torsional vibrations in a simple shaft. Wauer et al [P32] used the equations derived in reference P31 to investigate the response of a cracked shaft to periodic axial impulses. The coupling effects are confirmed to be of significant magnitude in this work. The paper concludes that the technique can be used for crack detection, but little is said about practical implementation or experimental work.

A number of papers [P33,P34,P35,P36] give theoretical treatments of discretized rotating shaft systems with no experimental or practical fieldwork. The work elaborates somewhat on the calculation techniques and inherent errors, but generally confirms the theoretical trends and practical experience of Scheibel [P29,P30].

Feldman and Seibold [P37] published a paper of particular interest. It has been established so far that all researchers agree that the vibration of a shaft is influenced by the presence of a crack. It is generally accepted that the change may be small and that the required signal or changes, at least for early detection of small cracks, may be masked by general background noise. Signal processing techniques are available in a number of fields to enhance the signal-to-noise ratio or to identify signal content of particular interest to the problem at hand.

Scheibel et al [P29,P30] were the first published work, found in the literature survey, where signal processing is reported in this field. Feldman and Seibold [P37] make use of advanced signal processing techniques combined with theoretical modelling. The Hilbert transform enables separation of the measured vibrations into two parts, describing the system behaviour for positive and negative displacements respectively. If not identical, the separated signals would identify the existence of a crack, depending on the characteristics of the signal traces.

The system uses a Kalman filter to predict the difference between the measured signal and a predicted response. The general understanding is that the Kalman filter merges a model predicted response with the general measurement noise. The model is used to predict system responses for a number of crack locations (hypothesis). All the hypotheses are tested through Kalman filters and the one with the smallest difference indicates the correct hypothesis, and crack location. Feldman further suggests that the crack depth can be determined by parameter estimation (supported by some experimentation). Personal communication with Feldman indicated that he is not aware of commercialised systems using these principles and that his interest is purely academic with the main emphasis on signal processing.

5.4 MATERIAL PROPERTIES

Fatigue and fracture assessment requires a wide range of material information specific to the material under consideration. While stress analysis plays a major role, successful modelling of the problem is strongly dependent on material characterisation. An extensive literature survey was performed to obtain suitable values and models for the purposes of this study.

The industry standard for LP turbine material is CrMoV. Although different manufacturers have slightly different concentrations of alloying elements, the family of materials exhibits similar fatigue properties [P1,P38,P39]. A typical chemical composition is 0.25% C, 1.6% Cr, 0.4% Mn, 3% Ni, 0.4% Mo and 0.1%V.

The analysis requires material properties for the crack growth law constants of equation 3.3.2, the material toughness, K_{IC}, and the fatigue threshold, ΔK_{th}.

5.4.1 Crack Growth Law Constants [T14,T14,T15,T16]

The crack growth law describes crack propagation as a function of cycles and stress intensity range. The most commonly used law is the Paris equation (3.3.2). Fatigue crack growth, like the threshold stress intensity, is influenced by a large number of factors including:

- temperature
- atmosphere i.e. steam, air etc.
- stress ratio
- load frequency
- variable amplitude loading
- multiaxial loading

Some researchers derived crack growth laws that are based on the Paris law, but modified to incorporate some of the above influences. In general the Paris law can be retained with the stress intensity range, ΔK, expressed as the effective stress intensity range, ΔK_{eff} (equation 5.4.1). The stress ratio, R, and multiaxial loads would be the only two influences on the stress intensity range while the other influences are accommodated in the constants.

$$\frac{da}{dN} = C(\Delta K_{eff})^n \qquad (5.4.1)$$

C and α are constants that are calibrated to experimental data.

5.4.1.1 Atmosphere

The atmosphere to which a structure is exposed can have a major influence on the crack growth rate. The atmosphere attacks the crack front by corrosion, oxidation and other chemical processes to accelerate and in some cases retards crack growth.

In practice, it is often difficult to assess the environmental influences because the atmosphere is not well quantified. The general guidelines in steam turbine engineering are to neglect environmental effects when dry steam conditions can be assumed.

5.4.1.2 Temperature

Temperature has an effect on fatigue crack growth for two reasons namely:

- high temperature can result in creep that will cause creep-fatigue interaction and accelerated crack growth [T15]
- the atmosphere is influenced by temperature (for example dry vs wet steam) and most corrosion processes like oxidation become more active at high temperature [P40]

In most cases, the growth law constants are modified to reflect fits to experimental data for a specific case.

5.4.1.3 Stress Ratio [P40]

The stress ratio, R, is defined as:

$$R = \frac{\sigma_{min}}{\sigma_{max}} = \frac{K_{min}}{K_{max}} \qquad (5.4.2)$$

Crack closure concepts are used to explain the influence of R. When the crack is subjected to a compressive load, the crack surfaces touch each other and the crack is closed. In this condition there would be no driving force to extend the crack surface.

A tensile force, normal to the crack surface, would result in the crack surfaces lifting away from each other. The crack front is exposed and has a driving force to extend the crack surface. The crack opening stress, σ_{op}, is defined as the stress that will just open the crack at the crack front. The opening stress is associated with an opening stress intensity, K_{op}, so that:

$$\Delta K_{eff} = (K_{max} - K_{op}) \qquad (5.4.3)$$

When the crack front is in tension, a small plastic zone develops so that the crack front is in residual compression when it is unloaded. In subsequent tensile load cycles, this residual compressive stress must first be overcome before the crack front is opened so that the opening stress is often a tensile stress larger than zero.

The stress ratio would also have an influence on temperature effects. A high mean stress would result in more creep so that the effect of creep-fatigue interaction becomes smaller. High mean stress also means that the crack is almost always open and exposed to environmental effects.

A number of researchers developed models to account for the stress ratio effects of which equation 5.4.4 is by far the most common.

Crooker [T12]: $$\frac{da}{dN} = C[1-R]^{-0.5}(\Delta K)^{\alpha} \qquad (5.4.4)$$

The method is reported to correlate well with experimental results.

5.4.1.4 Load Frequency [P40]

Load frequency effects have an influence when the cracked structure is exposed to an adverse environment such that corrosion and oxidation processes are present. If the frequency is high enough, none of these effects have time to attack the crack front between cycles.

5.4.1.5 Variable Amplitude Loading

Extreme load cycles in variable amplitude loading have the effect that the opening stress is modified due to crack tip plasticity. Changes in the opening stress influences the effective stress intensity range so that crack growth retardation or acceleration can occur.

5.4.1.6 Multiaxial Loading

Multiaxial or mixed mode loading is a complex subject and is often associated with multifaceted crack growth. Although net crack growth normally occurs in the direction of maximum principal stress fluctuation, the crack front behaviour and growth morphology are dependent on the ratios between the loading modes [P41,P42,P43].

Growth laws, supported by experimental data, are often derived for the specific load cases under consideration. In the case of a power generating steam turbine with shrunk on disks, a transverse crack would be subjected to a fluctuating mode I (bending) and a constant mode III (torsional) stress intensity.

The fatigue threshold for this case is of more importance than the growth law because of the high frequency. Once the threshold is exceeded, the crack will extend very rapidly so that the component is effectively at the end of its useful life. It was explained in section 5.3 that the only safeguard against catastrophic failure is on-line detection of the crack by vibration monitoring. Crack growth during barring operation is only a function of mode I loading, since no torsion is transmitted at this stage of operation.

5.4.1.7 Published Data

A number of sources published experimental results for turbine steels [P1,P38,P39,P40]. Table 5.2 gives a summary of the test conditions and the derived Paris equation constants.

Source	[P1]U*	[P1]L*	[P38]	[P39]	[P40]
Stress Ratio	0.1	0.1	0.1	0.1	?
C	3.04E-11	1.69E-11	2.59E-11	2.5911E-11	2.21E-11
n	2.7	2.6	2.5	2.8	2.7
Temperature	25	25	?	25	?
Atmosphere	?	?	?	Air	?
Frequency	?	?	?	1	?

Table 5.2: Constants for Paris equation for da/dN in m/cycle and ΔK in $MPa.m^{0.5}$
* Derived from upper and lower bound of graph

Although very little information is available on the results of reference P38, the same values were recommended by the manufacturer. Figure 5.7, which gives a graphical comparison of the references in table 5.2, shows that the constants of reference P38 forms an approximate lower bound curve.

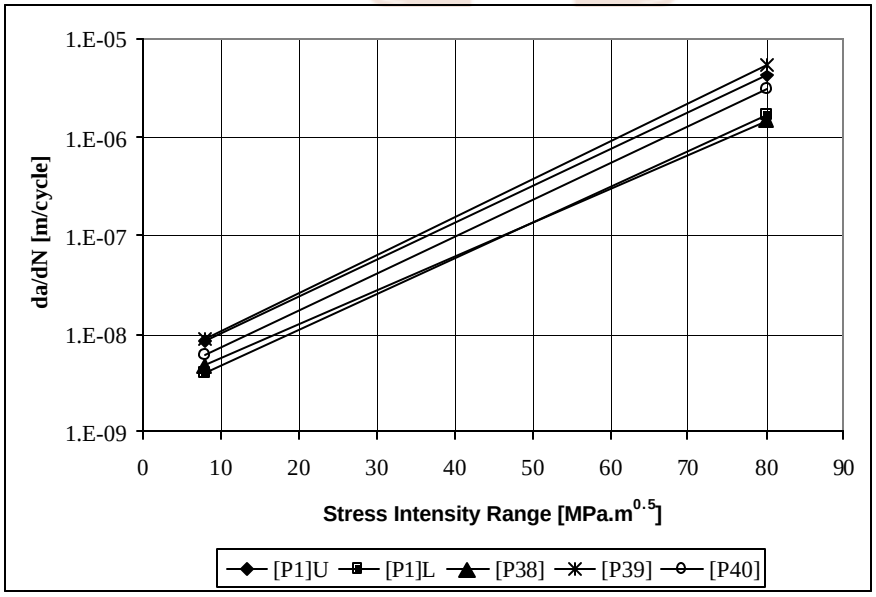

Figure 5.7: Graphical presentation of table 5.2

5.4.2 Material Toughness [U1]

The material limit for mode I stress intensity, toughness or K_{IC}, can be calculated from correlation formulae with the sharpy impact strength. Reference U1 has a wide range of impact test results on the turbine shafts under consideration. A conservative estimation of K_{IC} is given as 110 MPa.m$^{0.5}$ at 10 °C. Although this value can be used for barring conditions, the shaft operates at approximately 200 °C where the toughness would be higher at approximately 200 MPa.m$^{0.5}$.

A fracture criterion for multiaxial loading can be derived by substituting the energy criterion of equation 3.1.15 into equation 3.1.12 to derive an equivalent stress intensity that would result in the same energy release rate as the combined modes [P44]. The relationship is:

$$K_{eq} = \sqrt{K_I^2 + K_{II}^2 + \frac{K_{III}^2}{(1-\nu)}} \qquad (5.4.5)$$

5.4.3 Fatigue Threshold

Crack initiation is a complex field and researchers are still debating on how the ruling processes are defined [P45]. The initiation mechanisms will not be investigated in this section, but rather the factors influencing the fatigue threshold values.

Fatigue threshold is a material characteristic that depends on a number of factors. While general fatigue textbooks cover most factors, some are in a specialist area of application and need to be researched with the aid of open literature.

5.4.3.1 Stress Ratio vs. Grain Size

Two publications found on the subject of grain size, come to the general conclusion that fatigue-resistance increases with increasing grain size [P46,P47].

Lal [P46] presents a more comprehensive study which includes the effects of the stress ratio, R. Upper and lower bound ΔK_{th} values are postulated in Lal's studies for fine to coarse grained materials, the upper bound corresponding to coarse grained.

The difference is explained by the structure's sensitivity to R. All grain sizes have the same ΔK_{th} for high R ratios. Threshold values in fine-grained material are independent of R, while ΔK_{th} increases in coarse-grained materials for R ratios below 0.6.

Lal predicts an upper bound of 7.1 MPa.m$^{0.5}$ (at R = 0) and a lower bound of 2.8 MPa.m$^{0.5}$ (at R = 0.6), corresponding to an upper and lower bound grain size of

120 and 10 μm. The material in the case study has a grain size of approximately 90 μm, approaching the upper bound.

Lindley [P48] discusses the same topic, and demonstrated the same principles. Lindley quotes two equations for adjusting threshold values as a function of R as follows:

$$\Delta K_{th} = \Delta K_{th(R=0)} (1\text{-}R)^{\gamma} \qquad (5.4.6)$$

(γ = 0.71 for turbine steels)

for positive R. The second equation quoted by Lindley is:

$$\Delta K_{th} = \Delta K_{th(R=0)} f(R) \qquad (5.4.7)$$

with
$$f(R) = \sqrt{\frac{1-R}{1+R}} \quad \text{for } R \geq 0$$
$$f(R) = \frac{1-R}{1-\frac{R}{3}} \quad \text{for } R < 0$$

The effect of atmosphere is reported by Lindley [P48] and Lal [P49]. Threshold values measured in practice are often higher than predicted by the work in reference P46. The reason for that is oxide assisted crack closure or blunting. Reference P49 suggests that the upper bound of 7.1 MPa.m$^{0.5}$, reported in reference P46, should be adjusted to 8 MPa.m$^{0.5}$. This value corresponds well with measured values on turbine steels reported in reference P48.

5.4.3.2 Mixed Mode Loading

A number of predictive models were found on the influence of mixed mode loading on fatigue thresholds [P41,P50,P51,P52,P53]. Mixed mode I & II crack growth is treated along similar lines as mode I and III crack growth in most papers. Faceted crack growth was observed in all mixed mode experiments if the load ratios become favourable. To this end, some models make use of theoretical treatments of branched cracks, a concept that is often used for stress corrosion cracks.

The angle of the facets, relative to the stress field, is one of the essential parameters in all models. While a number of prediction-models are available, experimental observations from reference P50 show that the facet angles are best predicted by the maximum principal stress direction.

Yates [P50,P51] used crack opening displacement relations to predict a threshold criterion along geometrical arguments i.e. the threshold is reached when the geometrical sum of all displacements equals that of a critical value for mode I loading.

The resulting threshold criterion is:

$$\left[\frac{\Delta K_I}{\Delta K_{I,th}}\right]^2 \cos(\varphi) + 2.25\left[\frac{\Delta K_{III}}{\Delta K_{I,th}}\right]^2 \sin(\varphi) = 1 \qquad (5.4.8)$$

where φ is the facet angle. A modified or effective threshold, $\Delta K_{I,eff}$ can be calculated from equation 5.4.8 for a given K_{III} and $\Delta K_{I,th}$ as:

$$\Delta K_{I,eff} = \sqrt{\frac{\Delta K_{I,th}^2 - 2.25\Delta K_{III}^2 \sin(\varphi)}{\cos(\varphi)}} \qquad (5.4.9)$$

The fatigue threshold will decrease with increasing ΔK_{III} according to equation 5.4.9. Experimental results show that the effective stress intensity decreases with increasing static K_{III} [P42,P43]. It is to be expected that some of the mechanisms will change from static to fluctuating K_{III}, but most of the arguments used in the theoretical treatment of the problem would be equally valid for both cases.

Equation 5.4.8 compares well with a range of experimental results, but the tests were only conducted for relatively low ΔK_{III} values (smaller than ΔK_I). The fatigue tests were conducted on a fail/no-fail basis i.e. the fatigue threshold was not determined by incremental load variation. Although tests in reference P51 were conducted on a LP turbine steel, comparison to the results reported in reference P43 is not practically possible for the range of values used. Extrapolation of the trends in reference P51 to higher K_{III} values would give erroneous results compared to reference P43.

There is consensus amongst researchers that crack surface abrasion, faceted growth, increased crack tip plasticity and friction play an important role in mixed mode fatigue cracks. A faceted crack with a static mode III load would for example not be able to fully close when opened by a mode one load because of the mismatch in surface asperities. The Yates model does not account for these factors which is a likely reason for the incorrect predictions at higher static K_{III} loads.

The predictive models and associated experimental work focused mostly on proportional loading with cycling loads applied for both K_I and K_{III}. In the case of a steam turbine, the torsional load (K_{III}) is static, while the bending load (K_I) is cycling.

References P42 and P43 report on experimental results of mode I fatigue with steady mode III loading. The theoretical models, discussed earlier, do not predict the same results as experimentally determined for static K_{III}. The results of reference P43 are reproduced in figure 5.6. The tests were performed on pre-cracked samples opposed to the machined grooves in references P50 and P51. The fatigue threshold was determined by incrementally increasing ΔK_I with static K_{III} until crack growth occurs.

A number of attempts were made, by the author and a number of researchers in the quoted references, to derive a suitable model, based on practical and theoretical concepts, for the prediction of the data in figure 5.6. The assumptions around abrasive wear, friction and crack locking aspects were ultimately too crude to give reasonable predictions through the whole range of results. It was therefore decided to fit an empirical model for further use.

It is expected that abrasive effects will have a larger influence for low R values (-1) where the crack surfaces are in contact. The following relationship is postulated by the author:

$$\Delta K_{I,eff} = \Delta K_{I,th}(R) + \alpha(R) K_{III}^{\beta(R)} \qquad (5.4.10.a)$$

where α and β are functions of R.

The best fit to the experimental data in reference P43 was achieved with the following functions:

$$\alpha(R) = 0.00268\, e^{1.68115R}$$
$$\beta(R) = -0.94162\, R + 1.29662 \qquad (5.4.10.b)$$

Figure 5.8 shows the curves of equation 5.4.10 overlaid on the experimental data of reference P43. $\Delta K_{I,th}(R)$ is calculated from equation 5.4.7 with γ = 0.71 and $\Delta K_{I,th}(0)$ = 4.4. Equation 5.4.10 gives a good fit of the data and may serve as an appropriate model for a theoretical treatment of the general case to account for abrasive effects. Such a study falls outside the scope of this work.

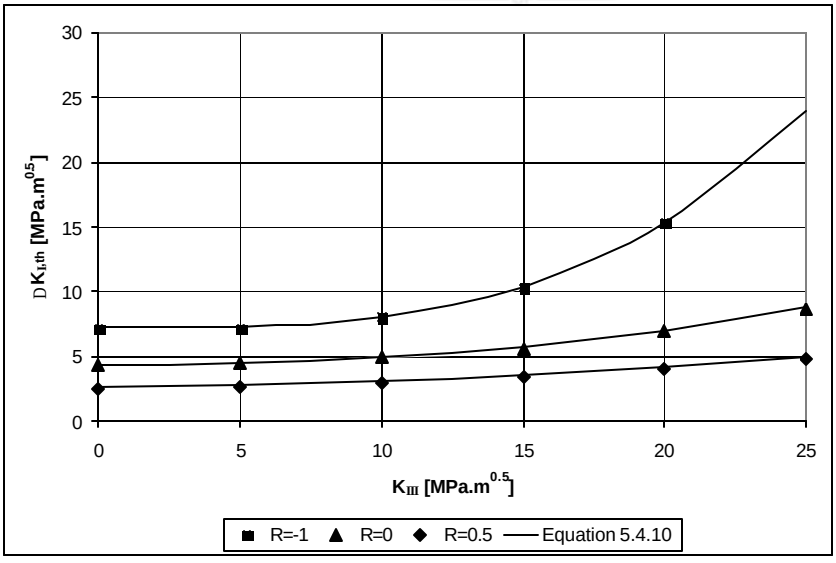

Figure 5.8: Curve of K_{III} influence on $\Delta K_{I,th}$
Numerical values were reproduced from reference P43

5.5 CONCLUSIONS

The general industry experience shows the following:

- Incidences of transverse cracking in steam turbines have been recorded.
- The critical crack size is large compared to the diameter of a rotor.
- Cracked rotors were detected by on-line crack vibration monitoring.
- General material behaviour is a well researched field and is covered by a number of papers.
- Published material data demonstrates the influence of a steady K_{III} on the fatigue threshold.

Although some influencing factors may warrant further investigation, sufficient knowledge and published data are available to enable evaluation of calculated parameters.